Hadronic effects on the $cc\bar{q}\bar{q}$ tetraquark state in relativistic heavy ion collisions

Juhee Hong,[1] Sungtae Cho,[2] Taesoo Song,[3,4] and Su Houng Lee[1]

[1]*Department of Physics and Institute of Physics and Applied Physics, Yonsei University, Seoul 03722, Korea*
[2]*Division of Science Education, Kangwon National University, Chuncheon 24341, Korea*
[3]*Frankfurt Institute for Advanced Studies, Johann Wolfgang Goethe Universität, Frankfurt am Main, Germany*
[4]*Institut für Theoretische Physik, Universität Gießen, Gießen, Germany*

We study the hadronic effects on the $cc\bar{q}\bar{q}$ tetraquark state by focusing on the $T_{cc}(1^+)$ meson during the hadronic stage of relativistic heavy ion collisions. We evaluate the absorption cross section of the T_{cc} meson by pions in the quasifree approximation, and investigate the time evolution of the T_{cc} abundance in the hadronic medium based on the effective volume and temperature of the hadronic phase at both the BNL Relativistic Heavy Ion Collider (RHIC) and the CERN Large Hadron Collider (LHC) modeled by hydrodynamic calculations with the lattice equation of state. We probe two possible scenarios for the structure of the T_{cc}, where it is assumed to be either a compact multiquark state or a larger sized molecular configuration composed of DD^*. Our numerical results suggest that the hadronic effects on the T_{cc} production are insignificant, and its final abundance depends on the initial yield of the T_{cc} produced from the quark-gluon plasma phase, which will depend on the assumed structure of the state.

I. INTRODUCTION

Exotic hadrons have been proposed to be important probes for understanding the fundamentals of the strong interaction in hadron physics [1,2]. The excitement in the subject restarted with the observation of $D_{sJ}(2317)$ [3] and $X(3872)$ [4], whose masses did not fit well within the conventional potential model approaches, and continues to the present day with the recent observation of $P_c(4380)^+$ and $P_c(4450)^+$ [5]. Detailed theoretical studies on the structure and properties of these states have been reported using various models [6–9]. Moreover, it has been argued that relativistic heavy ion collisions provide an excellent venue to produce some of these and previously proposed exotic states because they contain heavy quarks, which are profusely produced in these experiments [10–12]. Among many exotic hadrons, we focus here on the proposed doubly charmed tetraquark $T_{cc}(cc\bar{u}\bar{d} = DD^*)$ with the quantum number $I(J^P) = 0(1^+)$ [13–15].

There are several reasons why the T_{cc} is of particular interest. First of all, it is a flavor exotic tetraquark, which has never been observed before. Second, with the recent discovery of the doubly charmed baryon at CERN [16], the possibility of observing a similar doubly charmed hadron with the light quark replaced by a strongly correlated light anti-diquark seems quite plausible. Finally, analyzing the structure of this particle in the constituent quark model, one finds that this particle is the only candidate where there is a strong attraction in the compact configuration compared to two separated mesons. This is so because while previously observed exotic candidates such as the $X(3872)$ are composed of $q\bar{q}Q\bar{Q}$, where q, Q are light and heavy quarks respectively, the proposed T_{cc} state is composed of $QQ\bar{q}\bar{q}$ quarks. The latter quark structure favors a compact tetraquark configuration as the additional light anti-diquark structure $\bar{q}\bar{q}$ in the isospin zero channel provides an attraction larger than that for the two $Q\bar{q}$ in a separated meson configuration [17–19]. Hence, the T_{cc} is a unique multiquark candidate state that could be compact.

The measured yields of ground state particles and their ratios from relativistic heavy ion collisions can be well described by statistical models [20–22]. On the other hand, there are indications that yields for resonances with structures different from ground states deviate from the statistical model prediction [23,24]. In particular, it was argued that the yields of compact multiquark configurations would be an order of magnitude more suppressed compared to a molecular configuration or a usual hadron with the same quantum number and mass, if allowed, which should follow the statistical model prediction [10–12]. However, these results were obtained without considering the hadronic effects, which could change the initial production rate at the chemical freeze-out due to the interaction with other particles during the hadronic expansion before the kinetic freeze-out. The importance of this effect has been confirmed for states with large intrinsic width such as the K^*, which has been observed both at the BNL Relativistic Heavy Ion Collider (RHIC) and the CERN Large Hadron Collider (LHC) with yield ratios to the K that are systematically reduced compared to the statistical model predictions [25]. If the hadronic effects are large, the hope of using production yields to discriminate the structure of an exotic particle through its production could be problematic. In fact, for similar reasons, the hadronic effects of exotic candidates have been estimated for the $D_{sJ}(2317)$ [26] and $X(3872)$ [27,28].

In this work, we estimate the hadronic effects on the T_{cc} yields in heavy ion collisions to assess if the initial yields at the hadronization point are maintained, so that its structure can be discriminated. We also solve a hydrodynamic model based

on the lattice equation of state with and without viscosity, and parametrize the resulting time dependence of the temperature and volume during the hadronic phase at both RHIC and LHC that will be used in this and in similar future works.

This work is organized as follows. In Sec. II, we introduce a simplified hydrodynamic model to calculate and parametrize the time dependence of the temperature and volume of the hadronic phase at RHIC and LHC. In Sec. III, we discuss the hadronization in relativistic heavy ion collisions and the T_{cc} yields calculated in two possible scenarios, where the T_{cc} is either a compact configuration with suppressed yield estimated within the coalescence model or a weakly bound molecular configuration that should follow the statistical model prediction. In Sec. IV, the cross sections of the T_{cc} absorption by pions are calculated in the quasifree approximation. In Sec. V, the time evolution of the T_{cc} abundance is studied by solving the rate equation in the two possible scenarios. In Sec. VI, we give possible production final states that can be used to observe these states from heavy ion collisions. In Sec. VII, we discuss yields of doubly charmed baryons, comparing with the yields of the T_{cc} and D. Finally, we summarize our results in Sec. VIII.

II. HYDRODYNAMIC EQUATION FOR THE HADRONIC PHASE

Hydrodynamic equations are given by $\partial_\mu T^{\mu\nu} = 0$, where the energy-momentum tensor $T^{\mu\nu} = (e + p)u^\mu u^\nu - pg^{\mu\nu} + \pi^{\mu\nu}$ with e, p, u^μ, and $\pi^{\mu\nu}$ being, respectively, the energy density, pressure, four-velocity of flow, and the traceless symmetric shear tensor. For simplicity, we assume the boost invariance and consider central collisions, that is, symmetric expansion in the transverse plane. Then there are only two independent hydrodynamic equations [29],

$$\frac{1}{\tau}\partial_\tau(\tau T^{\tau\tau}) + \frac{1}{r}\partial_r(r T^{r\tau}) = -\frac{1}{\tau}(p + \tau^2\pi^{\eta\eta}), \quad (1)$$

$$\frac{1}{\tau}\partial_\tau(\tau T^{\tau r}) + \frac{1}{r}\partial_r(r T^{rr}) = \frac{1}{r}(p + r^2\pi^{\phi\phi}), \quad (2)$$

in the (τ, r, ϕ, η) coordinate system defined by

$$\tau = \sqrt{t^2 - z^2}, \quad \eta = \frac{1}{2}\ln\frac{t+z}{t-z},$$

$$r = \sqrt{x^2 + y^2}, \quad \phi = \tan^{-1}(y/x). \quad (3)$$

Nonvanishing energy-momentum tensors and shear tensors are respectively expressed as [29]

$$T^{\tau\tau} = (e + P_r)u_\tau^2 - P_r,$$
$$T^{\tau r} = (e + P_r)u_\tau u_r, \quad (4)$$
$$T^{rr} = (e + P_r)u_r^2 + P_r,$$

where $P_r \equiv p - \tau^2\pi^{\eta\eta} - r^2\pi^{\phi\phi}$ is the effective radial pressure, and

$$\pi^{\tau r} = v_r\pi^{rr},$$
$$\pi^{\tau\tau} = v_r\pi^{\tau r} = v_r^2\pi^{rr}, \quad (5)$$
$$\pi^{rr} = -\gamma_r^2(r^2\pi^{\phi\phi} + \tau^2\pi^{\eta\eta}),$$

with v_r being the radial velocity and the shear tensors $\pi^{\phi\phi}$ and $\pi^{\eta\eta}$ being the only independent ones. The components $\pi^{\phi\phi}$ and $\pi^{\eta\eta}$ are boost invariant in the radial direction and satisfy the following simplified Israel-Stewart equations:

$$(\partial_\tau + v_r\partial_r)\pi^{\eta\eta} = -\frac{1}{\gamma_r\tau_\pi}\left[\pi^{\eta\eta} - \frac{2\eta_s}{\tau^2}\left(\frac{\theta}{3} - \frac{\gamma_r}{\tau}\right)\right], \quad (6)$$

$$(\partial_\tau + v_r\partial_r)\pi^{\phi\phi} = -\frac{1}{\gamma_r\tau_\pi}\left[\pi^{\phi\phi} - \frac{2\eta_s}{r^2}\left(\frac{\theta}{3} - \frac{\gamma_r v_r}{r}\right)\right], \quad (7)$$

where

$$\theta = \partial u = \frac{1}{\tau}\partial_\tau(\tau\gamma_r) + \frac{1}{r}\partial_r(rv_r\gamma_r),$$

with η_s and τ_π being the shear viscosity and the relaxation time for the particle distributions, respectively. Furthermore, the condition $u_\mu(T_{;\nu}^{\nu\mu}) = 0$, where $T_{;\nu}^{\nu\mu}$ is the covariant derivative and the flow velocity $(u_\tau, u_r, u_\phi, u_\eta) = (\gamma/\cosh\eta, \gamma v_r, 0, 0)$ reduces to $(\gamma_r, \gamma_r v_r, 0, 0)$ with $\gamma_r = 1/\sqrt{1 - v_r^2}$ in midrapidity, leads to

$$\frac{1}{\tau}\partial_\tau(\tau s\gamma_r) + \frac{1}{r}\partial_r(rs\gamma_r v_r) = -\frac{1}{T}\left[\frac{u_\tau}{\tau}\tau^2\pi^{\eta\eta} + \frac{u_r}{r}r^2\pi^{\phi\phi} - (\partial_\tau u_\tau + \partial_r u_r)(r^2\pi^{\phi\phi} + \tau^2\pi^{\eta\eta})\right], \quad (8)$$

where $s = (e + p)/T$ is the local entropy density in the hot dense matter. Equation (8) shows that the total entropy is not conserved in the presence of nonzero shear tensors.

Integrating Eqs. (1) and (6)–(8) over the transverse plane, we have [30]

$$\partial_\tau(A\tau\langle T^{\tau\tau}\rangle) = -(p + \pi_\eta^\eta)A, \quad (9)$$

$$\frac{T}{\tau}\partial_\tau(A\tau s\langle\gamma_r\rangle) = -A\left\langle\frac{\gamma_r v_r}{r}\right\rangle\pi_\phi^\phi - \frac{A\langle\gamma_r\rangle}{\tau}\pi_\eta^\eta + \left[\partial_\tau(A\langle\gamma_r\rangle) - \frac{\gamma_R\dot{R}}{R}A\right](\pi_\phi^\phi + \pi_\eta^\eta), \quad (10)$$

$$\partial_\tau(A\langle\gamma_r\rangle\pi_\eta^\eta) - \left[\partial_\tau(A\langle\gamma_r\rangle) + 2\frac{A\langle\gamma_r\rangle}{\tau}\right]\pi_\eta^\eta = -\frac{A}{\tau_\pi}\left[\pi_\eta^\eta - 2\eta_s\left(\frac{\langle\theta\rangle}{3} - \frac{\langle\gamma_r\rangle}{\tau}\right)\right], \quad (11)$$

$$\partial_\tau(A\langle\gamma_r\rangle\pi_\phi^\phi) - \left[\partial_\tau(A\langle\gamma_r\rangle) + 2A\left\langle\frac{\gamma_r v_r}{r}\right\rangle\right]\pi_\phi^\phi = -\frac{A}{\tau_\pi}\left[\pi_\phi^\phi - 2\eta_s\left(\frac{\langle\theta\rangle}{3} - \left\langle\frac{\gamma_r v_r}{r}\right\rangle\right)\right], \quad (12)$$
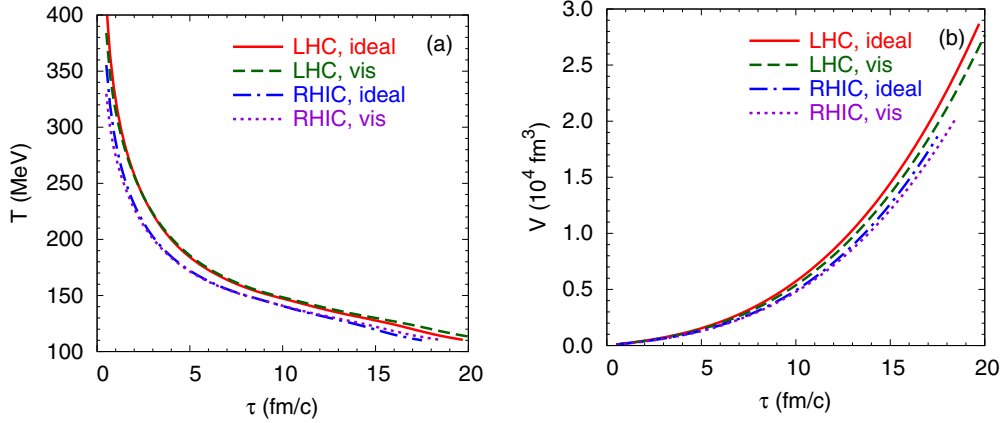
FIG. 1. (a) Temperature and (b) volume during the hadronic expansion for Pb+Pb collisions at $\sqrt{s_{NN}} = 2.76$ TeV at LHC and Au+Au collisions at $\sqrt{s_{NN}} = 200$ GeV at RHIC.

where $A = \pi R^2$ (R is the radius of nuclear matter), $\langle T^{\tau\tau} \rangle = \int dA\, T^{\tau\tau}/A = (e + p)\langle \gamma_r^2 \rangle - p$, $\langle u^{\tau} \rangle = \langle \gamma_r \rangle$, $\pi_{\eta}^{\eta} \equiv \tau^2 \pi^{\eta\eta}$, and $\pi_{\phi}^{\phi} \equiv r^2 \pi^{\phi\phi}$. We note that the total derivatives with respect to r disappear due to the boundary condition. Assuming that the radial flow velocity is a linear function of the radial distance from the center, that is, $\gamma_r v_r = \gamma_R \dot{R}(r/R)$, where $\dot{R} = \partial R/\partial \tau$ and $\gamma_R = 1/\sqrt{1 - \dot{R}^2}$,

$$\langle \gamma_r^2 \rangle = 1 + \frac{\gamma_R^2 \dot{R}^2}{2},$$

$$\langle \gamma_r^2 v_r^2 \rangle = \frac{\gamma_R^2 \dot{R}^2}{2},$$

$$\langle \gamma_r \rangle = \frac{2}{3\gamma_R^2 \dot{R}^2}(\gamma_R^3 - 1),$$

$$\left\langle \frac{\gamma_r v_r}{r} \right\rangle = \frac{\gamma_R \dot{R}}{R}. \tag{13}$$

Here, we make the assumption that nuclear matter has a definite boundary and e, s, and p are uniform inside. In real hydrodynamic simulations, the energy-momentum tensor is numerically calculated for all time-space cells leading to a different temperature for each cell so that the hypersurface for a constant temperature has a complex structure in the $xy\tau$ space. But at the same time, one finds that most of the points composing the hypersurface are located on a semiconstant τ plane [31]. That is why the blast wave model had been successful and widely used before sophisticated hydrodynamics became popular. This is the basis for our approximation.

We then numerically solve simultaneous Eqs. (9) to (12) by using the lattice equation of state [30,32]. The ratio of the shear viscosity to entropy density is taken to be $1/(4\pi)$ for quark-gluon plasma (QGP) [33], and ten times this value for hadron gas [34]. For the relaxation time τ_{π}, we assume $\eta/\tau_{\pi} = sT/3$ for both QGP and hadron gas [35]. The initial thermalization time for hydrodynamic simulations is assumed to be 0.5 fm/c, and the initial radius is given by the transverse area where the local temperature is above 150 MeV. Although the hydrodynamic approach is marginal in the hadron gas phase, it has successfully reproduced abundant experimental data from relativistic heavy ion collisions [36,37].

According to the hydrodynamic calculations, the temperature and volume during the hadronic phase for LHC (Pb+Pb collisions at $\sqrt{s_{NN}} = 2.76$ TeV) and RHIC (Au+Au collisions at $\sqrt{s_{NN}} = 200$ GeV) change with time as shown in Fig. 1. We now parametrize the results for the τ dependence of the volume and temperature using the following form [26,38]:

$$V(\tau) = \pi\left[R + v(\tau - \tau_C) + \frac{a}{2}(\tau - \tau_C)^2\right]^2 c\tau,$$

$$T(\tau) = T_C - (T_H - T_F)\left(\frac{\tau - \tau_H}{\tau_F - \tau_H}\right)^{\alpha} \quad \text{for } \tau > \tau_H, \tag{14}$$

with T_c (τ_c), T_H (τ_H), and T_F (τ_F) being the critical, hadronization, and kinetic freeze-out temperatures (times), respectively. In Eq. (14), we take $T_H = 156$ (162) MeV, $T_F = 115$ (119) MeV for LHC (RHIC), and $T_C = T_H$ by following the first scenario of Ref. [10]. R, v, a, and α have been treated as fitting parameters. All the parameters used in the model are given in Table I.

TABLE I. Parameters used in the phenomenological model of Eq. (14).

		$T_C = T_H$ (MeV)	T_F (MeV)	$\tau_C = \tau_H$ (fm/c)	τ_F (fm/c)	R (fm)	v (c)	a (c^2/fm)	α
LHC	ideal	156	115	8.1	18.3	12.1	0.70	0.022	0.95
	viscous	156	115	8.3	19.5	11.9	0.67	0.020	0.93
RHIC	ideal	162	119	6.1	15.1	9.9	0.59	0.030	0.85
	viscous	162	119	6.1	15.7	9.8	0.58	0.024	0.79

III. HADRONIZATION IN RELATIVISTIC HEAVY ION COLLISIONS

We assume that conventional hadrons such as π, D, and D^* are in chemical and thermal equilibrium when they are produced at the chemical freeze-out. The abundance of a particle in equilibrium is statistically given by [39]

$$
\begin{aligned}
N_i^{eq}(\tau) &= g_i \gamma_i V(\tau) \int \frac{d^3 \boldsymbol{p}}{(2\pi)^3} f(\boldsymbol{p}) \\
&= \frac{1}{2\pi^2} g_i \gamma_i m_i^2 V(\tau) T(\tau) K_2\left(\frac{m_i}{T(\tau)}\right),
\end{aligned}
\quad (15)
$$

where $g_i = (2S_i + 1)(2I_i + 1)$ is the spin and isospin degeneracy and γ_i is the fugacity. In the second line, the Boltzmann distribution $f(\boldsymbol{p}) = \exp[-\sqrt{\boldsymbol{p}^2 + m_i^2}/T(\tau)]$ has been used and K_2 is the modified Bessel function of the second kind. For simplicity we ignore the correction term to $f(\boldsymbol{p})$ for shear viscosity. Since the production and annihilation cross sections of charm quarks are small [40–42], the number of charm quarks is conserved during the time evolution of the hadronic matter. From the total number of charm quarks, $N_c = 11\,(4.1)$ [10], the charm fugacity is determined as $\gamma_c = 51\,(22)$ for LHC (RHIC). Here the charm fugacity is slightly different from that in Ref. [10] because we use only D, D^*, D_s, and D_s^* to saturate the charm quarks as in Eq. (28). By following Refs. [26,28], the number of pions at RHIC is set to be 926 at the kinetic freeze-out. For that purpose, we introduce a pion chemical potential with effective fugacity of 1.4 and use the same factor at LHC. This effect is to include the feed-down contributions from excited states such as the omega, delta, and K^*. Although these pions will only have a limited contribution to the absorption during the hadronic phase, we will include them in the calculation to allow for the maximum effect.

If the T_{cc} is of a molecular configuration composed of a weakly bound DD^*, the production yield is expected to follow the statistical model prediction as the production yield of light nuclei do so. In such a case, the number of the doubly charmed T_{cc} is given by Eq. (15) with γ_c^2, $V(\tau_H)$, and $T(\tau_H)$ for the fugacity, volume, and temperature, respectively. On the other hand, if the T_{cc} is a compact multiquark state with the size of a usual hadron, then the production yield would be suppressed compared to the statistical model prediction. The production yields have been estimated by the coalescence model, whose parameters have been fitted to reproduce the ground state hadron yields [10]. The two cases are summarized in Table II. Throughout this paper, we use the average masses $m_\pi = 137.3$ MeV, $m_D = 1867.2$ MeV, and $m_{D^*} = 2008.6$ MeV [43].
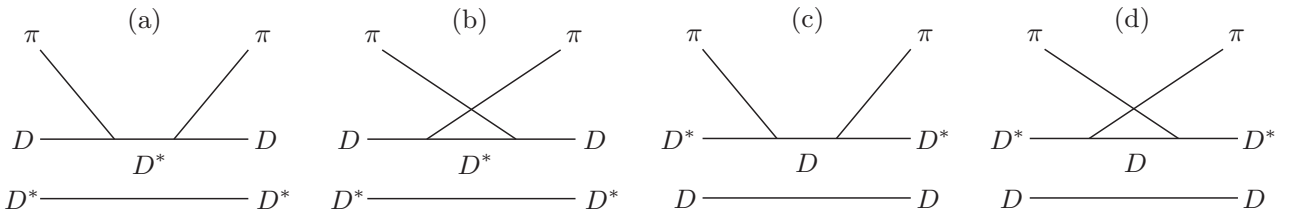
TABLE II. The T_{cc} yields at hadronization.

	molecular	compact multiquark
LHC	2.0×10^{-3}	1.1×10^{-4}
RHIC	5.1×10^{-4}	5.0×10^{-5}

IV. T_{cc} ABSORPTION CROSS SECTIONS

The T_{cc} can be produced or destroyed by interacting with other comoving particles during the hadronic expansion stage. Since pions are the most abundant particles with small mass, the interaction with them is the main contribution to the T_{cc} abundance. In this section, we calculate the absorption cross sections of the T_{cc} by pions in the quasifree approximation.

The quasifree approximation has been used previously to estimate the dissociation of charmonia by partons [44]. The approximation was shown to be valid when the binding energies of charmonia are small at high temperature, and c and $\bar{c}$ quarks inside charmonia can be treated like quasifree particles [45] (see Appendix A for the details). In fact, for the charmonium case, it can be seen that an exact next-to-leading order QCD calculation allowing for the compact size gives a similar result for the thermal width [46] as that obtained using the quasifree approximation when the process involves the same number of initial and final states. Here, we estimate the dissociation cross section of the T_{cc} by pions by estimating the D and D^* components of the T_{cc} in two possible scenarios under the quasifree approximation.

In the quasifree approximation, the cross section of $T_{cc} + \pi \to D + D^* + \pi$ can be evaluated by adding the elastic scattering $D + \pi \to D + \pi$ and $D^* + \pi \to D^* + \pi$ (see Fig. 2). For the effective interaction vertices, we use the following interaction Lagrangian [40]:

$$
\mathcal{L}_{\pi DD^*} = i g_{\pi DD^*} D^{*\mu} \boldsymbol{\tau} \cdot (\bar{D} \partial_\mu \boldsymbol{\pi} - \partial_\mu \bar{D} \boldsymbol{\pi}) + \text{H.c.}, \quad (16)
$$

where $\boldsymbol{\tau}$ are the Pauli matrices, $\boldsymbol{\pi}$ is the pion isospin triplet, and $D = (D^0, D^+)$ and $D^* = (D^{*0}, D^{*+})$ are the pseudoscalar and vector charm meson doublets, respectively. The meson coupling $g_{\pi DD^*}$ is determined from the $D^* \to D\pi$ decay width

$$
\Gamma_{D^* \to D\pi} = \frac{g_{\pi DD^*}^2 p_{cm}^3}{2\pi m_{D^*}^2}, \quad (17)
$$

where p_{cm} is the momentum in the center of mass frame. By comparing with the experimental data, the full width $\Gamma_{D^* \to D\pi} = 83.4$ keV [43], we obtain $g_{\pi DD^*} \simeq 7.8$.

FIG. 2. Diagrams contributing to the T_{cc} abundance. In the quasifree approximation, (a) and (b) correspond to the elastic scattering $D + \pi \to D + \pi$, and (c) and (d) to $D^* + \pi \to D^* + \pi$.

TABLE III. $2 \to 2$ processes contributing to the spin and isospin averaged cross section of Eq. (22). With the effective Lagrangian of Eq. (16), the matrix elements involve the factor $2^{N(\pi^{\pm})/2}$ in Eqs. (19) and (21).

Process	Diagram	Process	Diagram
$D^+\pi^0 \to D^+\pi^0$	(a)+(b)	$D^{*+}\pi^0 \to D^{*+}\pi^0$	(c)+(d)
$D^+\pi^0 \to D^0\pi^+$	(a)+(b)	$D^{*+}\pi^0 \to D^{*0}\pi^+$	(c)+(d)
$D^+\pi^- \to D^+\pi^-$	(a)	$D^{*+}\pi^- \to D^{*+}\pi^-$	(c)
$D^+\pi^- \to D^0\pi^0$	(a)+(b)	$D^{*+}\pi^- \to D^{*0}\pi^0$	(c)+(d)
$D^+\pi^+ \to D^+\pi^+$	(b)	$D^{*+}\pi^+ \to D^{*+}\pi^+$	(d)
$D^0\pi^+ \to D^0\pi^+$	(a)	$D^{*0}\pi^+ \to D^{*0}\pi^+$	(c)
$D^0\pi^+ \to D^+\pi^0$	(a)+(b)	$D^{*0}\pi^+ \to D^{*+}\pi^0$	(c)+(d)
$D^0\pi^0 \to D^0\pi^0$	(a)+(b)	$D^{*0}\pi^0 \to D^{*0}\pi^0$	(c)+(d)
$D^0\pi^0 \to D^+\pi^-$	(a)+(b)	$D^{*0}\pi^0 \to D^{*+}\pi^-$	(c)+(d)
$D^0\pi^- \to D^0\pi^-$	(b)	$D^{*0}\pi^- \to D^{*0}\pi^-$	(d)

The scattering amplitude of the process $D(p_1) + \pi(p_2) \to D(p_3) + \pi(p_4)$ is then given as

$$\mathcal{M}_{D\pi \to D\pi} = \mathcal{M}^{(a)} + \mathcal{M}^{(b)}, \tag{18}$$

where

$$\mathcal{M}^{(a)} = \frac{2^{N(\pi^{\pm})/2} g_{\pi DD^*}^2}{s - m_{D^*}^2} \left[-g^{\mu\nu} + \frac{(p_1 + p_2)^\mu (p_1 + p_2)^\nu}{m_{D^*}^2} \right]$$
$$\times (p_1 - p_2)_\mu (p_3 - p_4)_\nu,$$

$$\mathcal{M}^{(b)} = \frac{2^{N(\pi^{\pm})/2} g_{\pi DD^*}^2}{u - m_{D^*}^2} \left[-g^{\mu\nu} + \frac{(p_1 - p_4)^\mu (p_1 - p_4)^\nu}{m_{D^*}^2} \right]$$
$$\times (p_1 + p_4)_\mu (p_2 + p_3)_\nu. \tag{19}$$

Here, $N(\pi^{\pm})$ is the number of charged pions involved in initial and final states of the process (see Table III).

For $D^*(p_1) + \pi(p_2) \to D^*(p_3) + \pi(p_4)$, we have

$$\mathcal{M}_{D^*\pi \to D^*\pi} = \mathcal{M}^{(c)} + \mathcal{M}^{(d)}, \tag{20}$$

with

$$\mathcal{M}^{(c)} = -\frac{2^{N(\pi^{\pm})/2} g_{\pi DD^*}^2 \epsilon_1^\mu \epsilon_3^{*\nu}}{s - m_D^2} (p_1 + 2p_2)_\mu (p_3 + 2p_4)_\nu,$$

$$\mathcal{M}^{(d)} = -\frac{2^{N(\pi^{\pm})/2} g_{\pi DD^*}^2 \epsilon_1^\mu \epsilon_3^{*\nu}}{u - m_D^2} (-p_1 + 2p_4)_\mu (2p_2 - p_3)_\nu. \tag{21}$$

In the center of mass frame, the spin and isospin averaged cross section is

$$\sigma = \frac{1}{64\pi^2 g_1 g_2 s} \frac{|\boldsymbol{p}_f|}{|\boldsymbol{p}_i|} \int d\Omega \sum_{S,I} |\mathcal{M}|^2 F^4, \tag{22}$$

where g_1 and g_2 are the degeneracies of initial particles, $\boldsymbol{p}_i$ ($\boldsymbol{p}_f$) is the spatial momentum of initial (final) particles, and the summation is over the spins and isospins of both initial and final particles. The relevant processes are listed in Table III. At each interaction vertex, we have used the following form factors:

$$F = \frac{\Lambda^2}{\Lambda^2 + (\omega^2 - m_{ex}^2)} \quad \text{and} \quad \frac{\Lambda^2}{\Lambda^2 + \boldsymbol{q}^2} \tag{23}$$

for the s and u channels, respectively. Here, the cutoff $\Lambda = 1.0$ GeV is used, m_{ex} is the mass of the exchanged particle, ω is the total energy of incoming particles in the s channel, and $\boldsymbol{q}$ is the momentum transfer in the u channel in the center of mass frame. As the molecular configuration is expected to be of a larger object than the compact case, we have also varied the cutoff from 1 to 0.5 GeV for the molecular configuration and from 1 to 1.5 GeV for the compact case in the estimates for the LHC experiment. Using the form factors, the cross sections do not increase with the total center-of-mass energy.

To take into account the thermal effects, we define $\langle \sigma_{ab \to cd} v_{ab} \rangle$, the product of the cross section of two-body scattering ($ab \to cd$) and the relative velocity between initial particles, $v_{ab} = \sqrt{(p_a \cdot p_b)^2 - m_a^2 m_b^2}/(E_a E_b)$, averaged over the thermal momentum distributions of initial particles [47,48]:

$$\langle \sigma_{ab \to cd} v_{ab} \rangle(\tau) = \frac{\int d^3 \boldsymbol{p}_a d^3 \boldsymbol{p}_b \, f_a(\boldsymbol{p}_a) f_b(\boldsymbol{p}_b) \, \sigma_{ab \to cd} v_{ab}}{\int d^3 \boldsymbol{p}_a d^3 \boldsymbol{p}_b \, f_a(\boldsymbol{p}_a) f_b(\boldsymbol{p}_b)}$$

$$= \left[4 \left(\frac{m_a}{T(\tau)} \right)^2 \left(\frac{m_b}{T(\tau)} \right)^2 K_2 \left(\frac{m_a}{T(\tau)} \right) K_2 \left(\frac{m_b}{T(\tau)} \right) \right]^{-1} \int_{z_0} dz \, \sigma(\sqrt{s} = z T(\tau))$$

$$\times \left[z^2 - \left(\frac{m_a + m_b}{T(\tau)} \right)^2 \right] \left[z^2 - \left(\frac{m_a - m_b}{T(\tau)} \right)^2 \right] K_1(z), \tag{24}$$

where $z_0 = \max[(m_a + m_b)/T(\tau), (m_c + m_d)/T(\tau)]$. It should be noted, however, that we are approximating $\sigma_{T_{cc}\pi \to DD^*}$ by $\sigma_{D\pi \to D\pi}$ and $\sigma_{D^*\pi \to D^*\pi}$. Hence, when taking the thermal distribution, the distribution $f_a(\boldsymbol{p}_a)$ should be that of the T_{cc}. Furthermore, the threshold should also involve that of $m_D + m_{D^*} \to m_{T_{cc}}$. This amounts to taking $m_a = m_c = m_{T_{cc}}$ instead of m_D or m_{D^*}. The same approximation will be taken when calculating the inverse process. The derivation of this formula is given in Appendix B.

Figure 3 shows the cross sections and the thermally averaged ones of the elastic scattering $D(D^*) + \pi \to D(D^*) + \pi$.
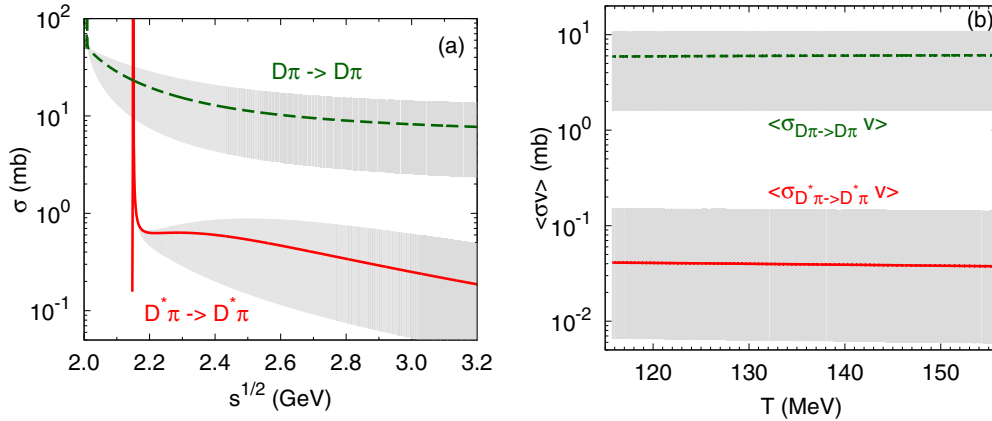
FIG. 3. (a) The cross sections as functions of the total center of mass energy and (b) the thermally averaged cross sections contributing to the absorption of the T_{cc} by pions. The shaded regions represent the cutoff dependence $\Lambda = 0.5-1.5$ GeV, the larger cutoff being the upper boundary.

The cross section of the s channel in the process $D + \pi \to D + \pi$ has a peak near the threshold energy $\sqrt{s_0} = m_D + m_\pi$ since $m_D + m_\pi \approx m_{D^*}$. Similarly, the cross section of the u channel in $D^* + \pi \to D^* + \pi$ diverges near $\sqrt{s_0} = m_{D^*} + m_\pi$.

V. TIME EVOLUTION OF THE T_{cc} ABUNDANCE

We consider the time evolution of the T_{cc} abundance governed by (see Appendix B)

$$
\frac{dN_{T_{cc}}(\tau)}{d\tau} = \langle \sigma_{T_{cc}\pi \to DD^*\pi} v_{T_{cc}\pi}\rangle(\tau) n_\pi(\tau)
$$
$$
\times \left[-N_{T_{cc}}(\tau) + N_{T_{cc}}^{eq}(\tau) \frac{N_D(\tau) N_{D^*}(\tau)}{N_D^{eq}(\tau) N_{D^*}^{eq}(\tau)} \right],
$$
(25)

where $n_\pi(\tau) = N_\pi(\tau)/V(\tau)$ and the superscript eq denotes the corresponding number in equilibrium. In the quasifree approximation, the absorption of the T_{cc} can be taken into account by using the two-body scattering $D(D^*) + \pi \to D(D^*) + \pi$,

$$
\langle \sigma_{T_{cc}\pi \to DD^*\pi} v_{T_{cc}\pi}\rangle(\tau)
$$
$$
= c_1 \langle \sigma_{D\pi \to D\pi} v_{T_{cc}\pi}\rangle(\tau) + c_1 \langle \sigma_{D^*\pi \to D^*\pi} v_{T_{cc}\pi}\rangle(\tau), \quad (26)
$$

where the factor c_1 will depend on the configuration of the T_{cc} for which we will consider the following two cases:

(1) *Compact configuration*: A compact configuration is expected when the T_{cc} is composed dominantly of a color triplet $\bar{q}\bar{q}$ state and a color antitriplet cc state [13,14]. Then the decomposition into two $c\bar{q}$ states will result in the color decomposition given as [17]

$$
T_{cc} = \frac{1}{\sqrt{3}}(D_1 D_1^*) - \sqrt{\frac{2}{3}}(D_8 D_8^*), \quad (27)
$$

where D_1, D_8 respectively denote the singlet and octet components of the $c\bar{q}$ color state. Hence, due to the coupling to color singlet states, we will take $c_1 = \frac{1}{3}$.

(2) *Molecular configuration*: If the diquark correlation is not strong enough, the T_{cc} could be a molecular

configuration of D, D^* coming from the long range pion exchange [15,18,49]. For this case we take $c_1 = 1$.

The production term of Eq. (25) has three bodies in the initial state, and we have approximated it using the equilibrium condition as derived in Appendix B.

To obtain the abundance of the T_{cc}, we have solved the rate equation (25) with the initial yields $N_{T_{cc}}(\tau_H)$ given in Table II. By using the equilibrium distributions for $N_D(\tau)$ and $N_{D^*}(\tau)$, the numerical results are shown in Fig. 4. Here we have used the time dependencies obtained by ideal hydrodynamic calculations. Those obtained using viscous hydrodynamics give almost the same results. In the first term of Eq. (25), the absorption rate of the T_{cc} is approximately 0.06 c/fm because $\langle \sigma_{D\pi \to D\pi} v\rangle(\tau) \sim 6$ mb in Fig. 3(b) and $n_\pi(\tau) \sim 0.1$ fm^{-3}. This alone would lead to about 45% reduction of the abundance as the typical lifetime of the hadronic phase is 10 fm/c. On the other hand, the production rate is approximately $O(10^{-4})$ smaller than the absorption rate, which can be seen easily from the factor $N_{T_{cc}}^{eq}(\tau)/[N_D^{eq}(\tau)N_{D^*}^{eq}(\tau)]$. Hence, its contribution
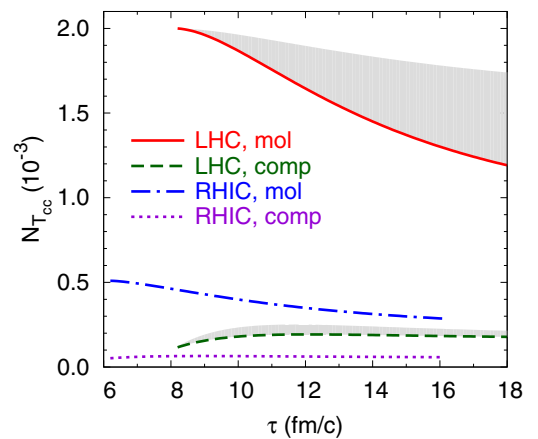

FIG. 4. The expected time evolution of the T_{cc} abundance in Pb+Pb collisions at $\sqrt{s_{NN}} = 2.76$ TeV at LHC and Au+Au collisions at $\sqrt{s_{NN}} = 200$ GeV at RHIC. The shaded regions represent the results obtained by varying the cutoff from 1 to 0.5 GeV (1.5 GeV) for a molecular (compact multiquark) configuration.
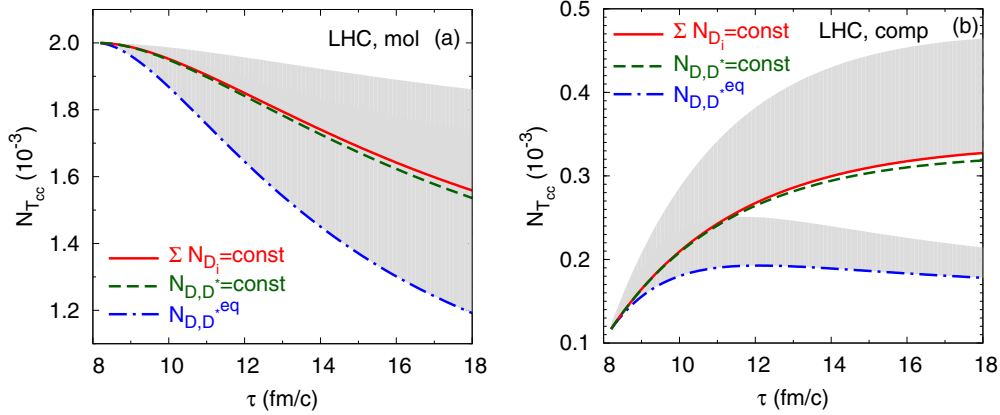
FIG. 5. $N_{D,D^*}(\tau)$ dependence on the T_{cc} yields for (a) molecular and (b) compact configurations. The shaded regions represent the results obtained by varying the cutoff from 1 to 0.5 GeV (1.5 GeV) for molecular (compact multiquark) configurations.

becomes important only at high density when the numbers of D, D^* mesons are large. Effectively, the production depends on the relative abundance between $N_{T_{cc}}(\tau)$ and $N_{T_{cc}}^{eq}(\tau)$. For a molecular configuration, while $N_{T_{cc}}(\tau_H) = N_{T_{cc}}^{eq}(\tau_H)$, the equilibrium number decreases and hence the number of the T_{cc} decreases (less than 42%) with time. For a compact multiquark state with relatively small initial yields, the number of the T_{cc} increases but it remains an order of magnitude smaller than a molecular configuration as the cross section for production is as small as that for the absorption. The dependence on the cutoff parameter is shown by the shaded regions in Fig. 4. By lowering (raising) Λ for a molecular (compact multiquark) configuration, the expected numbers of T_{cc} grow for both configurations, but the cutoff dependent hadronic effects on a multiquark state are smaller due to the factor c_1.

The final yield of the T_{cc} depends strongly on the initial number at hadronization. Because of the large initial yield, the expected abundance of the T_{cc} at LHC is larger than that at RHIC. These results mean that the numbers of charm quarks and the T_{cc} produced from the quark-gluon plasma phase are important to determine the final abundance of the T_{cc}. We can conclude that for both the RHIC and LHC experiments, the large difference between the coalescence and statistical expectations, obtained assuming that the T_{cc} is a compact multiquark or molecular configuration, remains until the kinetic freeze-out.

We have also considered the case that D and D^* are not in chemical equilibrium. This is important as the total number of charm quarks is expected to be conserved during the hadronic phase. The processes where the numbers of D, D^* change are related to Eq. (25), where the absorption of the T_{cc} is related to the production of D, D^* and its inverse relation. However, instead of solving the coupled rate equations involving charmed hadrons, we will consider two extreme cases:

(1) After the chemical freeze-out, the numbers of D and D^* will be assumed to be constant.
(2) We will assume that the inelastic cross sections involving light hadrons are large so that the ratios of charmed hadrons follow the equilibrium ones until the kinetic freeze-out point. While extreme, such a scenario

seems to be consistent with the experimental findings for the K^*/K ratios from heavy ion collisions [50]. This scenario is easily implemented by allowing the fugacity $\gamma_c(\tau)$ to depend on time during the hadronic phase using the following condition:

$$\sum_{D_i = D, D^*, D_s, D_s^*} N_{D_i}(\tau)$$
$$= \gamma_c(\tau)\left[N_D^0(\tau) + N_{D^*}^0(\tau) + N_{D_s}^0(\tau) + N_{D_s^*}^0(\tau) \right],$$
$$= \text{total number of charm quarks,} \tag{28}$$

where $N_{D_i}^0(\tau)$'s are the equilibrium numbers given in Eq. (15) without the fugacity. Once $\gamma_c(\tau)$ is obtained, one can assume that the individual numbers also satisfy the similar relations at each time,

$$N_D(\tau) = \gamma_c(\tau) N_D^0(\tau),$$
$$N_{D^*}(\tau) = \gamma_c(\tau) N_{D^*}^0(\tau). \tag{29}$$

This will guarantee that the charm-anticharm annihilation processes are small such that the total numbers of charmed and anticharmed mesons remain constant throughout the hadronic phase.

The correct numbers would be somewhere between the two extreme cases.

Figure 5 shows the results for the two cases. When D and D^* are not in equilibrium, the T_{cc} is more likely to be produced for both molecular and compact configurations. In fact, the number of the T_{cc} is largest in the limit of Eq. (28). However, we still find that even in this extreme limit, the abundance for a compact multiquark state at the end of the hadronic phase remains a factor of 5 smaller than that for a molecular configuration.

It is still possible that the total wave function of T_{cc} has both a compact and a molecular configuration. In such a case, the formation of T_{cc} would proceed through both the compact and molecular components with weighting factors determined from its wave function. Then, the production would be somewhere between our results determined by the molecular and compact cases. As an order of estimate, neglecting the production from the compact configuration, the final production yield would then be reduced from the molecular estimate to the

fraction of its component in the wave function. Given the range of yields in LHC as shown in Fig. 5, a clear distinction would only be possible if the fraction of the molecular configuration is of the order of 50%. If the fraction is larger (smaller), it would be hard to distinguish it from the case where the configuration is purely molecular (compact).

VI. FINAL STATES

Here we will list the possible final states that could be measured to reconstruct the T_{cc} from heavy ion collisions. The model calculations at present vary on the exact value of the binding energy. Therefore, we will probe all possibilities [51]. It should be noted that one could also look at the charge conjugate final states and search for $T_{\bar{c}\bar{c}}$ mesons:

(1) $m_{T_{cc}} \geqslant m_D + m_{D^*}$: In this case,

$$T_{cc} \to \text{(a) } D^0 + D^{*+} \text{ or (b) } D^+ + D^{*0} \text{ or}$$
$$\text{(c) } D^+ + D^+ + \pi^-. \tag{30}$$

As $D^{*+} \to D^0 + \pi^+$ and $D^0 \to K^- + \pi^+$, (a) can be reconstructed with vertex detectors. D^{*0} in (b) may not be easy to detect directly.

(2) $m_D + m_{D^*} \geqslant m_{T_{cc}} \geqslant m_D + m_D + m_\pi$: This would be the most likely case for a compact multiquark state. Then, the virtual D^{*+} component can decay into $D^0 + \pi^+$ so that a detectable final state would be

$$T_{cc} \to D^0 + D^0 + \pi^+. \tag{31}$$

The final state involving $T_{cc} \to D^0 + D^+ + \pi^0$ would be harder to identify. We note that the final state of Eq. (31) is not distinguishable from that of Eq. (30) (a).

(3) $m_{T_{cc}} \leqslant m_D + m_D + m_\pi$: In this case, the virtual D^* component should also decay into $D + \pi$ so that a detectable final state would be

$$T_{cc} \to D^0 + K^- + \pi^+ + \pi^+ \text{ or } D^+ + K^- \\ + \pi^+ + \pi^+ + \pi^-. \tag{32}$$

Among all the above cases, Eqs. (30) (c) ($D^+ + D^+ + \pi^-$) and (31) ($D^0 + D^0 + \pi^+$) seem to be the most probable cases to reconstruct the T_{cc}.

VII. Ξ_{cc} DECAY

Observing Ξ_{cc}^{++} in heavy ion collisions through the final states $\Lambda_c^+ + K^- + \pi^+ + \pi^+$, as was used by the LHCb Collaboration, would be a useful starting point before searching for T_{cc} in these collisions. For this purpose, we estimate the production rate for Ξ_{cc} in heavy ion collisions. The Ξ_{cc} state is expected to have a hyperfine partner $S = 3/2$ with a mass of about 64 MeV above its $S = 1/2$ ground state [52]. This state can not decay into a pion and its ground state due to the small mass difference. However, it can decay electromagnetically and contribute as a feed-down to the total Ξ_{cc} production. We will estimate the production of both states using the statistical model. Ξ_{cc} has a mass of 3621 MeV, as observed by the LHCb Collaboration, with $S = I = 1/2$. The Ξ_{cc}^* is expected to have a mass of around 3685 MeV with $S = 3/2$ and $I = 1/2$. In Table IV, we show the expected yields of $\Xi_{cc} = (\Xi_{cc}^{++} + \Xi_{cc}^+)$

TABLE IV. Yields of doubly charmed baryons and the D meson in midrapidity. The feed-down from Ξ_{cc}^* to the Ξ_{cc} production is not included. The numbers for T_{cc} are at the kinetic freeze-out point obtained with $\Lambda = 1$ GeV while those for the others are at the hadronization point.

	D	Ξ_{cc}	Ξ_{cc}^*	$T_{cc}(\text{mol})$	$T_{cc}(\text{comp})$
LHC	3.7	1.2×10^{-2}	1.7×10^{-2}	1.2×10^{-3}	1.8×10^{-4}
RHIC	1.3	3.0×10^{-3}	4.1×10^{-3}	3.0×10^{-4}	5.9×10^{-5}

together with those of $D = (D^0 + D^+)$ and T_{cc}, which will serve as a reference point for accessing the feasibility to measure these particles in a heavy ion collision.

VIII. SUMMARY

We have investigated the hadronic effects on the $cc\bar{q}\bar{q}$ tetraquark state by focusing on the T_{cc} multiplicity during the hadronic phase at RHIC and LHC. In particular, we have considered the absorption by pions and the inverse process within the quasifree approximation, where the T_{cc} is considered as a D, D^* state with appropriate coupling strength depending on whether it has a compact multiquark or molecular structure. We have extracted the time dependence of the volume and temperature for the hadronic phase for both the RHIC and LHC from the hydrodynamic calculations based on the lattice equation of state with or without viscosity. By solving the rate equation for the T_{cc} and estimating the changes for the D and D^* number, we have calculated how much the structure dependent initial number changes during the hadronic phase. Furthermore, we have also considered all the possible final states that could be measured to reconstruct the T_{cc} from heavy ion collisions. Among all the cases, we find $D^+ + D^+ + \pi^-$ and $D^0 + D^0 + \pi^+$ to be the most probable cases to reconstruct the T_{cc}.

For a molecular configuration, where the initial number of the T_{cc} is expected to follow the statistical model prediction, the absorption effect is larger than production and reduces the abundance by about 42%. When a compact tetraquark structure is assumed, the initial number estimated from a coalescence model is an order of magnitude smaller than that from the statistical model estimate, and hence production is larger. However, we find that due to the small cross section of about 6 mb, the rate of change is not large enough so that the initial order of magnitude difference in the assumed abundance is maintained at the end of the hadronic phase. This suggests that measuring the T_{cc} from heavy ion collisions could also tell us about the nature of its structure, which could either be a compact multiquark state or a loosely bound molecular configuration.

ACKNOWLEDGMENTS

APPENDIX A: $2 \to 3$ SCATTERING

Consider a process where two particles of momenta $q + k_1$ scatter into three particles of momenta $p_1 + p_2 + k_2$. The cross section is written as

$$\sigma_{\text{diss}} = \frac{1}{2E_q 2E_{k_1} v_{qk_1} g_q g_{k_1}} \int \frac{d^3 \boldsymbol{p}_2}{(2\pi)^3 2E_{p_2}} \frac{d^3 \boldsymbol{p}_1}{(2\pi)^3 2E_{p_1}} \frac{d^3 \boldsymbol{k}_2}{(2\pi)^3 2E_{k_2}} (2\pi)^4 \delta^4(p_1 + p_2 + k_2 - q - k_1)|\mathcal{M}|^2$$

$$= \int \frac{d^3 \boldsymbol{p}_2}{(2\pi)^3 2E_{p_2}} \int d^4 k \delta^4(k + p_2 - q) \frac{1}{2E_q 2E_{k_1} v_{qk_1}} (2E_k 2E_{k_1} v_{kk_1}) \frac{1}{2E_k 2E_{k_1} v_{kk_1} g_q g_{k_1}}$$

$$\times \int \frac{d^3 \boldsymbol{p}_1}{(2\pi)^3 2E_{p_1}} \frac{d^3 \boldsymbol{k}_2}{(2\pi)^3 2E_{k_2}} (2\pi)^4 \delta^4(p_1 + k_2 - k - k_1)|\mathcal{M}|^2. \tag{A1}$$

The matrix element is defined from

$$\mathcal{M} = \langle q, k_1 | p_2, p_1, k_2 \rangle, \tag{A2}$$

where each state is normalized as

$$\langle q | p \rangle = (2\pi)^3 2E_q \delta^3(\boldsymbol{q} - \boldsymbol{p}). \tag{A3}$$

The quasifree (QF) part is given as

$$\mathcal{M}_{QF} = \langle k, k_1 | p_1, k_2 \rangle. \tag{A4}$$

Quasifree approximation means that all the particles involved are on-shell. Therefore, we can approximate in the q rest frame $(\boldsymbol{q} = 0)$

$$|\mathcal{M}|^2 = \frac{g_q}{g_k} \left| \frac{\langle q | p_2, k \rangle}{\langle k | k \rangle} \right|^2 |\mathcal{M}_{QF}|^2 = \frac{g_q}{g_k} (2\pi)^3 2E_q \delta^3(\boldsymbol{p}_2 + \boldsymbol{k})|\mathcal{M}_{QF}|^2. \tag{A5}$$

If we allow small off-shell effects, as explicitly shown in Ref. [45], one can approximate the right-hand side of Eq. (A5) as follows:

$$|\mathcal{M}|^2 = \frac{g_q}{g_k} (2\pi)^3 2E_q |\psi(p)|^2 |\mathcal{M}_{QF}|^2, \tag{A6}$$

where $\psi(p)$ is the relative wave function of the bound state with $p \approx |\boldsymbol{p}_2| \approx |\boldsymbol{k}|$.

Substituting Eq. (A5) into Eq. (A1), we obtain

$$\sigma_{\text{diss}} = \int d^4 k \delta^4(k + p_2 - q) \frac{E_q}{E_{p_2}} \frac{1}{2E_q 2E_{k_1} v_{qk_1}} (2E_k 2E_{k_1} v_{kk_1})$$

$$\times \frac{1}{2E_k 2E_{k_1} v_{kk_1} g_q g_{k_1}} \int \frac{d^3 \boldsymbol{p}_1}{(2\pi)^3 2E_{p_1}} \frac{d^3 \boldsymbol{k}_2}{(2\pi)^3 2E_{k_2}} (2\pi)^4 \delta^4(p_1 + k_2 - k - k_1)|\mathcal{M}_{QF}|^2. \tag{A7}$$

We assume that q and p_2 are at rest and the resonance is barely bound so that $m_q/2 = m_k = m_{p_2}$. Then, we have

$$\sigma_{\text{diss}} = \frac{1}{2E_k 2E_{k_1} v_{kk_1} g_k g_{k_1}} \int \frac{d^3 \boldsymbol{p}_1}{(2\pi)^3 2E_{p_1}} \frac{d^3 \boldsymbol{k}_2}{(2\pi)^3 2E_{k_2}} (2\pi)^4 \delta^4(p_1 + k_2 - k - k_1)|\mathcal{M}_{QF}|^2 = \sigma_{QF}. \tag{A8}$$

Therefore, any addition of thermal factors related to external particles could be obtained by multiplying the corresponding thermal factors $f(\boldsymbol{p})$.

So far, we have assumed that the QF scattering occurs with only one constituent. If the interaction occurs with other particles independently, one can just sum the matrix elements. However, quantum mechanical effects with a specific form of the interaction are important when interference terms are to be taken care consistently. The interaction between particles 1,2 and a third particle 3 with a respective flavor matrix λ_i, can be written in general as

$$\lambda_1 \lambda_3 + \lambda_2 \lambda_3 = \frac{1}{2}\left[(\lambda_1 + \lambda_2 + \lambda_3)^2 - (\lambda_1 + \lambda_2)^2 - \lambda_3^2\right] = 0 \quad \text{if } (\lambda_1 + \lambda_2) = 0. \tag{A9}$$

That is, the cross section would be zero if there is no additional momentum difference in the vertex. A nonzero contribution arises when there is a derivative acting on the momentum difference between particle 1 and 2. In this case, the interaction will pick up a term proportional to the dipole of the system [45],

$$\lambda_1 \lambda_3 \partial \psi(p). \tag{A10}$$

After the momentum integral, the matrix element would be of order $O(1)$ as the typical momentum the derivative picks up would be inversely proportional to the size of the wave function. Therefore, the QF approximation would be good as an order-of-magnitude estimate of the cross section even when the total isospin of the bound state is zero.

APPENDIX B: RATE EQUATION

In the $2 \to 2$ case ($A + B \to C + D$), the interaction rate is given by

$$
\frac{dN}{V d\tau}(A + B \to C + D)
$$

$$
= g_A g_B \int \frac{d^3 \boldsymbol{p}_A}{(2\pi)^3} \frac{d^3 \boldsymbol{p}_B}{(2\pi)^3} f_A(\boldsymbol{p}_A) f_B(\boldsymbol{p}_B) v_{AB} \sigma_{A+B \to C+D}
$$

$$
= \int \frac{d^3 \boldsymbol{p}_A}{(2\pi)^3 2E_A} \frac{d^3 \boldsymbol{p}_B}{(2\pi)^3 2E_B} \frac{d^3 \boldsymbol{p}_C}{(2\pi)^3 2E_C} \frac{d^3 \boldsymbol{p}_D}{(2\pi)^3 2E_D} f_A(\boldsymbol{p}_A) f_B(\boldsymbol{p}_B)(2\pi)^4 \delta^{(4)}(p_A + p_B - p_C - p_D)|\mathcal{M}_{A+B \to C+D}|^2. \quad \text{(B1)}
$$

Generalizing the second line of the above equation to the $M \to N$ case,

$$
\frac{dN}{V d\tau}(A_1 + A_2 + \cdots + A_M \to B_1 + B_2 + \cdots + B_N) = \int \prod_{i=1}^{M} \frac{d^3 \boldsymbol{p}_{A_i}}{(2\pi)^3 2E_{Ai}} f_{A_i}(\boldsymbol{p}_{A_i}) \prod_{j=1}^{N} \frac{d^3 \boldsymbol{p}_{B_j}}{(2\pi)^3 2E_{Bj}} (2\pi)^4 \delta^{(4)}(p_{A1} + \cdots
$$

$$
+ p_{A_M} - p_{B1} - \cdots - p_{B_N})|\mathcal{M}_{A_1 + \cdots + A_M \to B_1 + \cdots + B_N}|^2. \quad \text{(B2)}
$$

Applying Eq. (B2) to our study, $T_{cc} + \pi \to D + D^* + \pi$ and $D + D^* + \pi \to T_{cc} + \pi$,

$$
\frac{dN}{V d\tau}(T_{cc} + \pi \to D + D^* + \pi) = \int \frac{d^3 \boldsymbol{p}_D}{(2\pi)^3 2E_D} \frac{d^3 \boldsymbol{p}_{D^*}}{(2\pi)^3 2E_{D^*}} \frac{d^3 \boldsymbol{p}_{\pi f}}{(2\pi)^3 2E_{\pi f}} \frac{d^3 \boldsymbol{p}_{T_{cc}}}{(2\pi)^3 2E_{T_{cc}}} \frac{d^3 \boldsymbol{p}_{\pi i}}{(2\pi)^3 2E_{\pi i}}
$$

$$
\times f(\boldsymbol{p}_{T_{cc}}) f(\boldsymbol{p}_{\pi i})(2\pi)^4 \delta^{(4)}(p_D + p_{D^*} + p_{\pi f} - p_{T_{cc}} - p_{\pi i})|\mathcal{M}_{T_{cc} + \pi \to D + D^* + \pi}|^2, \quad \text{(B3)}
$$

and

$$
\frac{dN}{V d\tau}(D + D^* + \pi \to T_{cc} + \pi) = \int \frac{d^3 \boldsymbol{p}_D}{(2\pi)^3 2E_D} \frac{d^3 \boldsymbol{p}_{D^*}}{(2\pi)^3 2E_{D^*}} \frac{d^3 \boldsymbol{p}_{\pi f}}{(2\pi)^3 2E_{\pi f}} \frac{d^3 \boldsymbol{p}_{T_{cc}}}{(2\pi)^3 2E_{T_{cc}}} \frac{d^3 \boldsymbol{p}_{\pi i}}{(2\pi)^3 2E_{\pi i}} f(\boldsymbol{p}_D) f(\boldsymbol{p}_{D^*}) f(\boldsymbol{p}_{\pi f})
$$

$$
\times (2\pi)^4 \delta^{(4)}(p_D + p_{D^*} + p_{\pi i} - p_{T_{cc}} - p_{\pi f})|\mathcal{M}_{D+D^*+\pi \to T_{cc}+\pi}|^2, \quad \text{(B4)}
$$

where π^i and π^f are incoming and outgoing pions.

Since the transition amplitude for $D + D^* + \pi \to T_{cc} + \pi$ is same as that for $T_{cc} + \pi \to D + D^* + \pi$, the change of the number of the T_{cc} is given by

$$
\frac{dN_{T_{cc}}}{V d\tau} = \int \frac{d^3 \boldsymbol{p}_D}{(2\pi)^3 2E_D} \frac{d^3 \boldsymbol{p}_{D^*}}{(2\pi)^3 2E_{D^*}} \frac{d^3 \boldsymbol{p}_{\pi f}}{(2\pi)^3 2E_{\pi f}} \frac{d^3 \boldsymbol{p}_{T_{cc}}}{(2\pi)^3 2E_{T_{cc}}} \frac{d^3 \boldsymbol{p}_{\pi i}}{(2\pi)^3 2E_{\pi i}}
$$

$$
\times (2\pi)^4 \delta^{(4)}(p_D + p_{D^*} + p_{\pi f} - p_{T_{cc}} - p_{\pi i})|\mathcal{M}_{T_{cc}+\pi \to D+D^*+\pi}|^2 [f(\boldsymbol{p}_D) f(\boldsymbol{p}_{D^*}) f(\boldsymbol{p}_{\pi f}) - f(\boldsymbol{p}_{T_{cc}}) f(\boldsymbol{p}_{\pi i})]. \quad \text{(B5)}
$$

The scattering cross section for $T_{cc} + \pi \to D + D^* + \pi$ is given by

$$
\sigma_{T_{cc}+\pi \to D+D^*+\pi} = \frac{1}{2E_{T_{cc}} 2E_{\pi i} v_{T_{cc}\pi i} g_{T_{cc}} g_\pi} \int \frac{d^3 \boldsymbol{p}_D}{(2\pi)^3 2E_D} \frac{d^3 \boldsymbol{p}_{D^*}}{(2\pi)^3 2E_{D^*}} \frac{d^3 \boldsymbol{p}_{\pi f}}{(2\pi)^3 2E_{\pi f}}
$$

$$
\times (2\pi)^4 \delta^{(4)}(p_D + p_{D^*} + p_{\pi f} - p_{T_{cc}} - p_{\pi i})|\mathcal{M}_{T_{cc}+\pi \to D+D^*+\pi}|^2. \quad \text{(B6)}
$$

(1) *Absorption*: We introduce the thermal averaged cross section defined in Eq. (24) in the text. Then, the absorption can be written as

$$
\frac{dN_{T_{cc}}}{V d\tau} = -\langle \sigma_{T_{cc}\pi \to DD^*\pi} v_{T_{cc}\pi} \rangle n_{T_{cc}} n_\pi, \quad \text{(B7)}
$$

where

$$
n = \frac{N}{V} = g \int \frac{d^3 \boldsymbol{p}}{(2\pi)^3} f(\boldsymbol{p}). \quad \text{(B8)}
$$

(2) *Production*: Instead of working out the three body cross section, using detailed balance, we will take it to be of the following form:

$$
\frac{dN_{T_{cc}}}{V d\tau} = \langle \sigma_{T_{cc}\pi \to DD^*\pi} v_{T_{cc}\pi} \rangle n_{T_{cc}}^{eq} \frac{n_D n_{D^*}}{n_D^{eq} n_{D^*}^{eq}} n_\pi. \quad \text{(B9)}
$$

Collecting the absorption and production terms,

$$\frac{dN_{T_{cc}}}{V d\tau} = \langle \sigma_{T_{cc}\pi \rightarrow DD^*\pi} v_{T_{cc}\pi} \rangle n_\pi \left(n_{T_{cc}}^{eq} \frac{n_D n_{D^*}}{n_D^{eq} n_{D^*}^{eq}} - n_{T_{cc}} \right). \tag{B10}$$

This is the rate equation we will be using in Eq. (25).

---

[1] R. L. Jaffe, Phys. Rev. D **15**, 267 (1977).
[2] R. L. Jaffe, Phys. Rev. D **15**, 281 (1977).
[3] B. Aubert *et al.* (BABAR Collaboration), Phys. Rev. Lett. **90**, 242001 (2003).
[4] S. K. Choi *et al.* (Belle Collaboration), Phys. Rev. Lett. **91**, 262001 (2003).
[5] R. Aaij *et al.* (LHCb Collaboration), Phys. Rev. Lett. **115**, 072001 (2015).
[6] E. S. Swanson, Phys. Rep. **429**, 243 (2006).
[7] M. B. Voloshin, Prog. Part. Nucl. Phys. **61**, 455 (2008).
[8] M. Nielsen, F. S. Navarra, and S. H. Lee, Phys. Rep. **497**, 41 (2010).
[9] N. Brambilla *et al.*, Eur. Phys. J. C **71**, 1534 (2011).
[10] S. Cho *et al.* (ExHIC Collaboration), Prog. Part. Nucl. Phys. **95**, 279 (2017).
[11] S. Cho, T. Furumoto, T. Hyodo, D. Jido, C. M. Ko, S. H. Lee, M. Nielsen, A. Ohnishi, T. Sekihara, S. Yasui, and K. Yazaki, (ExHIC Collaboration), Phys. Rev. Lett. **106**, 212001 (2011).
[12] S. Cho, T. Furumoto, T. Hyodo, D. Jido, C.M. Ko, S.H. Lee, M. Nielsen, A. Ohnishi, T. Sekihara, S. Yasui, and K. Yazaki, (ExHIC Collaboration), Phys. Rev. C **84**, 064910 (2011).
[13] S. Zouzou, B. Silvestre-Brac, C. Gignoux, and J. M. Richard, Z. Phys. C **30**, 457 (1986).
[14] H. J. Lipkin, Phys. Lett. B **172**, 242 (1986).
[15] A. V. Manohar and M. B. Wise, Nucl. Phys. B **399**, 17 (1993).
[16] R. Aaij *et al.* (LHCb Collaboration), Phys. Rev. Lett. **119**, 112001 (2017).
[17] W. Park and S. H. Lee, Nucl. Phys. A **925**, 161 (2014).
[18] T. Hyodo, Y. R. Liu, M. Oka, and S. Yasui, arXiv:1708.05169.
[19] S. Q. Luo, K. Chen, X. Liu, Y. R. Liu, and S. L. Zhu, Eur. Phys. J. C **77**, 709 (2017).
[20] P. Braun-Munzinger, D. Magestro, K. Redlich, and J. Stachel, Phys. Lett. B **518**, 41 (2001).
[21] A. Andronic, P. Braun-Munzinger, and J. Stachel, Nucl. Phys. A **772**, 167 (2006).
[22] J. Stachel, A. Andronic, P. Braun-Munzinger, and K. Redlich, J. Phys.: Conf. Ser. **509**, 012019 (2014).
[23] Y. Kanada-En'yo and B. Muller, Phys. Rev. C **74**, 061901 (2006).
[24] S. Cho, Phys. Rev. C **91**, 054914 (2015).
[25] J. Adam *et al.* (ALICE Collaboration), Phys. Rev. C **95**, 064606 (2017).
[26] L. W. Chen, C. M. Ko, W. Liu, and M. Nielsen, Phys. Rev. C **76**, 014906 (2007).

[27] S. Cho and S. H. Lee, Phys. Rev. C **88**, 054901 (2013).
[28] L. M. Abreu, K. P. Khemchandani, A. M. Torres, F. S. Navarra, and M. Nielsen, Phys. Lett. B **761**, 303 (2016).
[29] U. W. Heinz, H. Song, and A. K. Chaudhuri, Phys. Rev. C **73**, 034904 (2006).
[30] T. Song, K. C. Han, and C. M. Ko, Phys. Rev. C **83**, 024904 (2011).
[31] T. Song, W. Park, and S. H. Lee, Phys. Rev. C **84**, 054903 (2011).
[32] S. Borsanyi, G. Endrodi, Z. Fodor, A. Jakovac, S. D. Katz, S. Krieg, C. Ratti, and K. K. Szabo, J. High Energy Phys. 11 (2010) 077.
[33] P. K. Kovtun, D. T. Son, and A. O. Starinets, Phys. Rev. Lett. **94**, 111601 (2005).
[34] N. Demir and S. A. Bass, Phys. Rev. Lett. **102**, 172302 (2009).
[35] H. Song, Ph.D. thesis, The Ohio State University, 2009.
[36] P. F. Kolb, J. Sollfrank, and U. W. Heinz, Phys. Rev. C **62**, 054909 (2000).
[37] B. Schenke, S. Jeon, and C. Gale, Phys. Rev. C **82**, 014903 (2010).
[38] L. W. Chen, V. Greco, C. M. Ko, S. H. Lee, and W. Liu, Phys. Lett. B **601**, 34 (2004).
[39] P. Braun-Munzinger, K. Redlich, and J. Stachel, in *Quark Gluon Plasma 3*, edited by R. Hwa and X. N. Wang (World Scientific, Singapore, 2004), p. 491.
[40] Z. Lin and C. M. Ko, Phys. Rev. C **62**, 034903 (2000).
[41] W. Liu, C. M. Ko, and Z. W. Lin, Phys. Rev. C **65**, 015203 (2001).
[42] W. Liu and C. M. Ko, Phys. Lett. B **533**, 259 (2002).
[43] C. Patrignani *et al.* (Particle Data Group), Chin. Phys. C **40**, 100001 (2016), and 2017 update.
[44] L. Grandchamp and R. Rapp, Phys. Lett. B **523**, 60 (2001).
[45] T. Song, W. Park, and S. H. Lee, Phys. Rev. C **81**, 034914 (2010).
[46] Y. Park, K. I. Kim, T. Song, S. H. Lee, and C. Y. Wong, Phys. Rev. C **76**, 044907 (2007).
[47] P. Koch, B. Müller, and J. Rafelski, Phys. Rep. **142**, 167 (1986).
[48] C. M. Ko, X. N. Wang, B. Zhang, and X. F. Zhang, Phys. Lett. B **444**, 237 (1998).
[49] S. Ohkoda, Y. Yamaguchi, S. Yasui, K. Sudoh, and A. Hosaka, Phys. Rev. D **86**, 034019 (2012).
[50] S. Cho and S. H. Lee, Phys. Rev. C **97**, 034908 (2018).
[51] S. H. Lee, S. Yasui, W. Liu, and C. M. Ko, Eur. Phys. J. C **54**, 259 (2008).
[52] M. Karliner and J. L. Rosner, Phys. Rev. D **90**, 094007 (2014).